Nonlinear Analysis of Axially Loaded Concrete-Filled Tube Columns with Confinement Effect

Hsuan-Teh Hu, M.ASCE[1]; Chiung-Shiann Huang[2]; Ming-Hsien Wu[3]; and Yih-Min Wu[4]

Abstract: Proper material constitutive models for concrete-filled tube (CFT) columns are proposed and verified by the nonlinear finite element program *ABAQUS* against experimental data. The cross sections of the CFT columns in the numerical analysis are categorized into three groups, i.e., circular section, square section, and square section stiffened by reinforcing ties. Via the numerical analyses, it is shown that for circular CFT columns, the tubes can provide a good confining effect to the concrete especially when the width-to-thickness ratio D/t is small (say $D/t<40$). For square CFT columns, the tubes do not provide a large confining effect to the concrete especially when the width-to-thickness ratio B/t is large (say $B/t>30$). The confining effect of square CFT columns with reinforcing ties is enhanced by the use of reinforcing ties especially when the tie spacing is small and the tie number (or tie diameter) is large.

DOI: 10.1061/(ASCE)0733-9445(2003)129:10(1322)

CE Database subject headings: Columns; Nonlinear analysis; Axial loads; Confinement; Parameters.

Introduction

Concrete-filled tube (CFT) columns can provide excellent seismic resistant structural properties such as high strength, high ductility, and large energy absorption capacity. In addition to the enhancement in structural properties, a considerable amount of construction time can be reduced due to the prevention of permanent formwork. As a result, various research on CFT columns has been done in recent years (Furlong 1967; Knowles and Park 1969; Furlong 1974; Ge and Usami 1992; Ge and Usami 1994; Boyd, Cofer, and McLean 1995; Bradford 1996; Hajjar and Gourley 1996; Shams and Saadeghvaziri 1997; Uy 1998; Morino 1998; Schneider 1998; Zhang and Shahrooz 1999; Liang and Uy 2000; Bradford, Loh, and Uy 2002; Huang et al. 2002).

The enhancement of CFT columns in structural properties is due to the composite action between the constituent elements. The steel shell acts as longitudinal and transverse reinforcement. The shell also provides confining pressure to the concrete, which puts the concrete under a triaxial state of stress. On the other hand, the steel tube is stiffened by the concrete core. This can prevent the inward buckling of the steel tube, and increase the stability and strength of the column as a system. It is known that the ultimate strengths of CFT columns are influenced by their constituent material properties such as the compressive strength of the concrete and the yield strength of the steel. In addition, the ultimate strengths of CFT columns are also influenced by the concrete confining pressure and the geometric properties of the tubes such as the shape of the cross section, the width-to-thickness ratio, and the spacing and the diameter of the reinforcing ties.

The aim of this investigation is to employ the nonlinear finite element program *ABAQUS* (Hibbitt, Karlsson, and Sorensen 2000) to perform numerical simulations of CFT columns subjected to axial compressive loads. To achieve this goal, proper material constitutive models for steel reinforcing tie, steel tube, and concrete are proposed. Then the proposed material constitutive models are verified against experimental data of Schneider (1998) and Huang et al. (2002). Finally, the influence of the concrete confining pressure and the geometric properties of the columns on the uniaxial behavior of CFT columns are studied and discussed.

Material Properties and Constitutive Models

The cross sections of the CFT columns in this investigation can be categorized into three groups (Fig. 1), i.e., circular section (denoted by CU), square section (denoted by SU), and square section stiffened with steel reinforcing ties forming an octagonal shape (denoted by SS). The square tubes for SU sections were constructed by seam welding two U-shaped cold-formed steel plates. If stiffening was specified for SS sections, the tie bars were fillet welded to the U-shaped cold-formed steel plates before making the seam complete penetration groove welds (Huang et al. 2002). The materials used in the numerical analysis involve steel reinforcing tie (for SS section only), steel tube, and concrete. Constitutive models of these materials are proposed and discussed as follows.

Steel Reinforcing Tie

When the stress in the reinforcing tie exceeds the yield stress σ_y, the tie will exhibit plastic deformation. The stress-strain curve of

[1]Professor, Dept. of Civil Engineering, National Cheng Kung Univ., Tainan, Taiwan 701, R.O.C. E-mail: hthu@mail.ncku.edu.tw

[2]Associate Professor, Dept. of Civil Engineering, National Chiao Tung Univ., Hsinchu, Taiwan 30050, R.O.C.

[3]Research Assistant, Dept. of Civil Engineering, National Cheng Kung Univ., Tainan, Taiwan 701, R.O.C.

[4]Research Assistant, Dept. of Civil Engineering, National Cheng Kung Univ., Tainan, Taiwan 701, R.O.C.

Note. Associate Editor: Sherif El-Tawil. Discussion open until March 1, 2004. Separate discussions must be submitted for individual papers. To extend the closing date by one month, a written request must be filed with the ASCE Managing Editor. The manuscript for this paper was submitted for review and possible publication on January 3, 2002; approved on December 16, 2002. This paper is part of the ***Journal of Structural Engineering***, Vol. 129, No. 10, October 1, 2003. ©ASCE, ISSN 0733-9445/2003/10-1322–1329/$18.00.

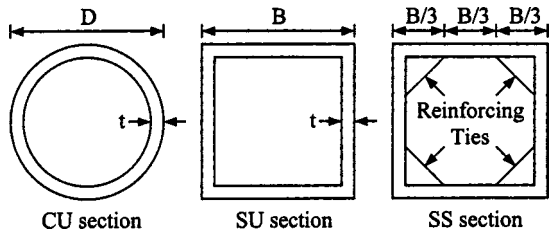

Fig. 1. Cross sections of CFT columns

the reinforcing tie is assumed to be elastic-perfectly plastic. The elastic modulus of the reinforcing tie E_S is assumed to be $E_S = 200$ GPa.

Steel Tube

In the analysis, the Poisson's ratio ν_S and the elastic modulus E_S of the steel tube are assumed to be $\nu_S = 0.3$ and $E_S = 200$ GPa. The uniaxial behavior of the steel tube is similar to reinforcing tie and thus can be simulated by an elastic-perfectly plastic model. When the steel tube is subjected to multiple stresses, a von Mises yield criterion F is employed to define the elastic limit, which is written as

$$F = \sqrt{3J_2} = \frac{1}{\sqrt{2}} \sqrt{(\sigma_1 - \sigma_2)^2 + (\sigma_2 - \sigma_3)^2 + (\sigma_3 - \sigma_1)^2} = \sigma_y \tag{1}$$

where J_2 = second stress invariant of the stress deviator tensor and σ_1, σ_2, and σ_3 = principal stresses. The response of the steel tube is modeled by an elastic-perfectly-plastic theory with associated flow rule. When the stress points fall inside the yield surface, the behavior of the steel tube is linearly elastic. If the stresses of the steel tube reach the yield surface, the behavior of the steel tube becomes perfectly plastic. Consequently, the steel tube is assumed to fail and can not resist any further loading.

Concrete

The Poisson's ratio ν_c of concrete under uniaxial compressive stress ranges from 0.15 to 0.22, with a representative value of 0.19 or 0.20 (ASCE 1982). In this study, the Poisson's ratio of concrete is assumed to be $\nu_c = 0.2$.

Let the uniaxial compressive strength and the corresponding strain of the unconfined concrete be f_c' and ε_c' (Fig. 2). The value

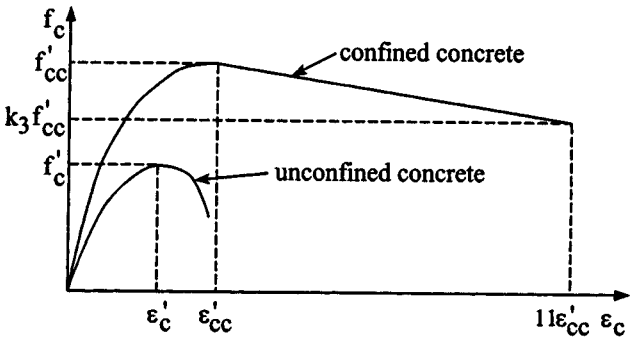

Fig. 2. Equivalent uniaxial stress-strain curve for concrete

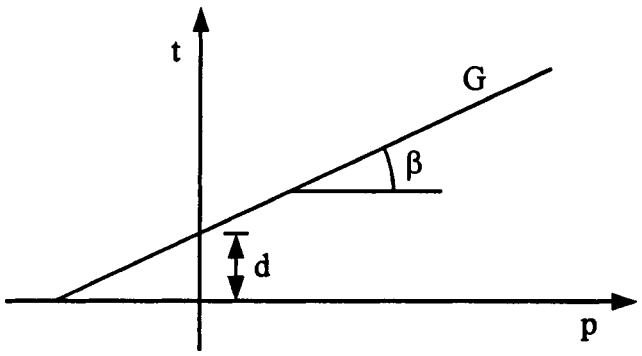

Fig. 3. Linear Drucker-Prager yield criterion for concrete

of ε_c' is usually around the range of 0.002 to 0.003. A representative value suggested by ACI Committee 318 (1999) and used in the analysis is $\varepsilon_c' = 0.003$.

When concrete is subjected to laterally confining pressure, the uniaxial compressive strength f_{cc}' and the corresponding strain ε_{cc}' (Fig. 2) are much higher than those of unconfined concrete. The relations between f_{cc}', f_c' and between ε_{cc}', ε_c' are estimated by the following equations (Mander, Priestley, and Park 1988)

$$f_{cc}' = f_c' + k_1 f_l \tag{2}$$

$$\varepsilon_{cc}' = \varepsilon_c' \left(1 + k_2 \frac{f_l}{f_c'} \right) \tag{3}$$

where f_l represents the confining pressure around the concrete core. The k_1 and k_2 are constants and can be obtained from experimental data. Meanwhile, the constants k_1 and k_2 were set as 4.1 and 20.5 based on the studies of Richart et al. (1928).

Because the concrete in the CFT columns is usually subjected to triaxial compressive stresses, the failure of concrete is dominated by the compressive failure surface expanding with increasing hydrostatic pressure. Hence, a linear Drucker-Prager yield criterion G (Fig. 3) is used to model the yield surface of concrete, which is expressed as

$$G = t - p \tan\beta - d = 0 \tag{4}$$

where

$$p = -(\sigma_1 + \sigma_2 + \sigma_3)/3 \tag{5a}$$

$$d = \left(1 - \frac{\tan\beta}{3} \right) f_{cc}' \tag{5b}$$

$$t = \frac{\sqrt{3J_2}}{2} \left[1 + \frac{1}{K} - \left(1 - \frac{1}{K} \right) \left(\frac{r}{\sqrt{3J_2}} \right)^3 \right] \tag{5c}$$

$$r = \left[\frac{9}{2} (S_1^3 + S_2^3 + S_3^3) \right]^{1/3} \tag{5d}$$

and S_1, S_2, and S_3 are principal stress deviators. The constants K and β are material parameters determined from experimental data. In the analysis, $K = 0.8$ and $\beta = 20°$ are used (Wu 2000).

The response of the concrete is modeled by an elastic-plastic theory with associated flow and isotropic hardening rule. When plastic deformation occurs, there should be a certain parameter to guide the expansion of the yield surface. A commonly used approach is to relate the multidimensional stress and strain conditions to a pair of quantities, namely, the effective stress f_c and effective strain ε_c, such that results obtained following different loading paths can all be correlated by means of the equivalent

J. Struct. Eng. 2003.129:1322-1329.

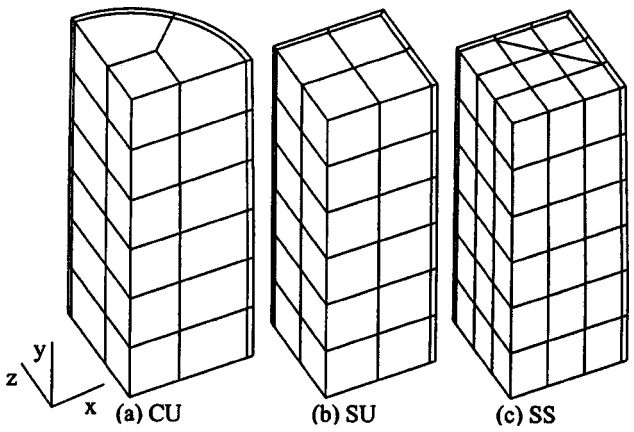

Fig. 4. Finite element mesh for CFT columns

uniaxial stress-strain curve. The stress-strain relationship proposed by Saenz (1964) has been widely adopted as the uniaxial stress-strain curve for concrete and it has the following form:

$$f_c = \frac{E_c \varepsilon_c}{1 + (R + R_E - 2)\left(\frac{\varepsilon_c}{\varepsilon'_{cc}}\right) - (2R - 1)\left(\frac{\varepsilon_c}{\varepsilon'_{cc}}\right)^2 + R\left(\frac{\varepsilon_c}{\varepsilon'_{cc}}\right)^3} \quad (6)$$

where

$$R = \frac{R_E(R_\sigma - 1)}{(R_\varepsilon - 1)^2} - \frac{1}{R_\varepsilon}, \quad R_E = \frac{E_c \varepsilon'_{cc}}{f'_{cc}}$$

and $R_\sigma = 4$, $R_\varepsilon = 4$ may be used (Hu and Schnobrich 1989). The initial modulus of elasticity of concrete E_c is highly correlated to its compressive strength and can be calculated with reasonable accuracy from the empirical equation (ACI 1999)

$$E_c = 4{,}700\sqrt{f'_{cc}} \text{ MPa} \quad (7)$$

In the analysis, Eq. (6) is taken as the equivalent uniaxial stress-strain curve for concrete when the concrete strain ε_c is less than ε'_{cc} (Fig. 2). When $\varepsilon_c > \varepsilon'_{cc}$, a linear descending line is used to model the softening behavior of concrete. If k_3 is defined as the material degradation parameter, the descending line is assumed to be terminated at the point where $f_c = k_3 f'_{cc}$ and $\varepsilon_c = 11\varepsilon'_{cc}$.

Generally, the parameters f_l and k_3 should be provided in order to completely define the equivalent uniaxial stress-strain relation. These two parameters apparently depend on the width-to-thickness ratio (D/t or B/t), cross-sectional shape, and stiffening mean. Consequently, their appropriate values are determined by matching the numerical results with experimental results via parametric study.

Finite Element Model for Concrete-Filled Tubes Columns

Due to symmetry, only one eighth of the CFT column is analyzed (Fig. 4). Symmetric boundary conditions are enforced on the symmetric planes, which are $u = 0$ on the plane normal to the x-axis, $w = 0$ on the plane normal to the z-axis, and $v = 0$ on the bottom surface normal to the y-axis. The top surface of the column is fixed with $u = w = 0$ but allows displacement to take place in the y direction. The corners of CFT with square sections are assumed to be exact 90° and corner radii are not considered. The uniform compressive loading in the y direction is applied to the top surface of the column directly. In the finite element mesh, both the concrete core and the steel tube are modeled by 27-node solid elements (three degrees of freedom per node). For the SS section, the steel reinforcing tie is modeled by three-node truss elements.

The interaction between the concrete and the steel tube is modeled by special nine-node interface elements. The nodes of concrete and steel tube are connected by using the interface elements that require matching meshes on the two bodies. The elements can model infinitesimal sliding and friction (Hibbitt, Karlsson, and Sorensen 2000) between the concrete and the steel tube. The friction coefficient used in all the analyses is 0.25. Through the interface elements, the contact surfaces between the concrete and the steel tube are allowed to separate but not to penetrate each other.

A convergent study of the mesh has been done by the author (Wu 2000) using various element sizes for both circular and square CFT columns. It is shown that the results of the circular CFT column with 30 (5×6) elements [Fig. 4(a)] are almost identical to those with 192 (16×12) elements. Similarly, the results of square CFT columns with 48 (8×6) elements [Fig. 4(b)] are almost identical to those with 135 (15×9) elements. Since mesh refinement has very little influence on the numerical results, the coarse meshes shown in Fig. 4 are used through out the analyses.

Numerical Analysis

In this section, the experimental data from Schneider (1998) and Huang et al. (2002) are used to verify and calibrate the proposed material model for CFT columns. For convenience, each specimen in the analysis has an individual designation, involving two English letters followed by a series of numbers (Table 1). The first letter represents the cross-sectional shape of the specimen (C and S for circular and square, respectively). The second letter, S or U, denotes a specimen with or without stiffening ties, respectively. Meanwhile, the three numbers following the English letters denote the width-to-thickness ratio (D/t or B/t). For stiffened specimen, the last three numbers before the parentheses represent the center-to-center spacing between the steel reinforcing ties in terms of millimeters. Finally, the parenthesized number is the reinforcing bar number of the steel tie.

Simulations of Concrete-Filled Tube Columns with CU Section

The results of numerical simulations for CFT columns with a CU section are given in Table 2 and the curves of axial force versus axial strain for these columns are plotted against the experiment data in Fig. 5. Generally, the numerical results show very good agreement with the experimental data. It can be observed that both the lateral confining pressure f_l and the material degradation parameter k_3 decrease with the increasing of width-to-thickness ratio D/t. When the D/t ratio is small (i.e., the tube thickness is relatively thick compared with the diameter of concrete), the steel tubes provide strong lateral support to the concrete core. As a result, the lateral confining pressure f_l usually achieves a very large value (say 8 MPa for the CU-022 column). In addition, the material degradation parameter k_3 may be equal to 1 (e.g., CU-022 and CU-040), which means the concrete strength does not degrade beyond the ultimate point. On the other hand, when the D/t ratio is large (i.e., the tube thickness is relatively thin compared with the diameter of concrete), the steel tubes provide weak lateral support to the concrete core. As a result, the lateral con-

J. Struct. Eng. 2003.129:1322-1329.

Table 1. Geometry and Material Properties of Concrete-Filled Tube Columns

Column number	D or B (mm)	t (mm)	D/t or B/t	Length (mm)	Steel tube f_y (MPa)	Concrete f'_c (MPa)	Steel tie f_y (MPa)	Tested by
CU-022	140	6.5	22	602	313.0	23.80	—	Schneider (1998)
CU-040	200	5.0	40	840	265.8	27.15	—	Huang et al. (2002)
CU-047	140	3.0	47	602	285.0	28.18	—	Schneider (1998)
CU-070	280	4.0	70	840	272.6	31.15	—	Huang et al. (2002)
CU-100	300	3.0	100	900	232.0	27.23	—	Schneider (1998)
CU-150	300	2.0	150	840	341.7	27.23	—	Huang et al. (2002)
SU-017	127	7.47	17	609.6	347.0	23.80	—	Schneider (1998)
SU-022	127	5.67	22	609.6	312.0	23.80	—	Schneider (1998)
SU-029	127	4.34	29	609.6	357	26.00	—	Schneider (1998)
SU-040	200	5.0	40	840	265.8	27.15	—	Huang et al. (2002)
SU-070	280	4.0	70	840	272.6	31.15	—	Huang et al. (2002)
SU-150	300	2.0	150	840	341.7	27.27	—	Huang et al. (2002)
SS-040-050(3)	200	5.0	40	840	265.8	27.15	410.9	Huang et al. (2002)
SS-040-050(4)	200	5.0	40	840	265.8	27.15	386.0	Huang et al. (2002)
SS-040-100(4)	200	5.0	40	840	265.8	27.15	386.0	Huang et al. (2002)
SS-070-093(2)	280	4.0	70	840	272.6	30.49	588.6	Huang et al. (2002)
SS-070-093(3)	280	4.0	70	840	272.6	30.49	615.3	Huang et al. (2002)
SS-070-093(4)	280	4.0	70	840	272.6	29.18	511.1	Huang et al. (2002)
SS-070-140(3)	280	4.0	70	840	272.6	29.84	615.3	Huang et al. (2002)
SS-070-140(4)	280	4.0	70	840	272.6	28.52	511.1	Huang et al. (2002)
SS-070-187(3)	280	4.0	70	840	272.6	29.18	615.3	Huang et al. (2002)
SS-070-187(4)	280	4.0	70	840	272.6	29.84	511.1	Huang et al. (2002)
SS-150-050(2)	300	2.0	150	840	341.7	24.00	735.8	Huang et al. (2002)
SS-150-100(2)	300	2.0	150	840	341.7	25.21	735.8	Huang et al. (2002)

fining pressure f_l usually has a very small value (say 0.3 MPa for the CU-150 column). In addition, the material degradation parameter k_3 may also have a lower value (say 0.6 for the CU-150 column). The behaviors of CFT columns with CU sections are highly influenced by the parameter k_3 of concrete. When $k_3=1$ (e.g., CU-022 and CU-040), the axial force-axial strain curves of the CFT columns do not show a degrading effect. However, when $k_3<1$, the axial force-axial strain curves of the CFT columns do show a degrading effect. This degrading phenomenon is more prominent with a smaller value of k_3.

Figs. 6(a and b) show the values of f_l/f_y and k_3 versus D/t ratio for CFT columns with the CU section, respectively. From the results of numerical simulations, two empirical equations may be proposed for f_l/f_y as follows:

$$f_l/f_y=0.043646-0.000832(D/t) \quad (21.7\leqslant D/t\leqslant 47) \quad (8a)$$

$$f_l/f_y=0.006241-0.0000357(D/t) \quad (47\leqslant D/t\leqslant 150) \quad (8b)$$

Due to limited test data, Eqs. (8*a*) and (8*b*) are not obtained by the least square method. Instead, they are formed by two straight lines connecting the data points at $D/t=22$, 47 and $D/t=47$, 150 [Fig. 6(a)]. For the parameter k_3, another two empirical equations may be proposed as follows:

$$k_3=1 \qquad (21.7\leqslant D/t\leqslant 40) \qquad (9a)$$

$$k3=0.0000339(D/t)2-0.010085(D/t)+1.3491 \qquad (40\leqslant D/t\leqslant 150) \quad (9b)$$

in which Eq. (9*a*) is a horizontal line connecting the data points at $D/t=22$, 40. Equation (9*b*) is a parabola passing through the data points at $D/t=40$, 150 with its vertex being the point $D/t=150$ [Fig. 6(b)].

Figs. 7(a and d) show the deformation shapes of CU-040 and CU-150 columns at the values of axial compressive strains very close to 0.025. It can be observed that these columns deform laterally in the radial direction. This lateral deformation for a column with larger D/t ratio is larger than that with smaller D/t ratio, especially in the middle section of the column (bottom of the finite element mesh). Because the confining pressure is uniformly applied to the concrete in all the radial directions, the concrete core and steel tube contact entirely to each other and no local buckling of the tube takes place. In addition to the lateral direction, confinement may also have a longitudinal effect, as recognized by research on a RC confinement model (El-Tawil and Deierlein 1999).

Simulations of Concrete-Filled Tubes Columns with SU Section

The results of numerical simulations for CFT columns with SU sections are again given in Table 2 and the curves of axial force versus axial strain for these columns are plotted against the experimental data in Fig. 8. Generally, the numerical results show good agreement with the experimental data. Similarly to the columns with CU section, both the lateral confining pressure f_l and the material degradation parameter k_3 decrease with increasing values of width-to-thickness ratio B/t. When the B/t ratio is small, f_l and k_3 tend to be large due to the lateral confinement from the steel tube. When the B/t ratio is large, f_l and k_3 tend to be small due to the lack of lateral support from the tube. Again, the behavior of CFT columns with a SU section is highly influenced by the parameter k_3 of concrete. When k_3 is large (say $0.7<k_3<1$), the axial force-axial strain curves of the CFT col-

J. Struct. Eng. 2003.129:1322-1329.

Table 2. Results of Numerical Analyses

Column number	Failure strength (kN)		Error (%)	f_l (MPa)	f_l/f_y	k_3
	Experiment	Analysis				
CU-022	1666.0	1628.0	2.30	8.00	0.0256	1.00
CU-040	2016.9	2024.0	0.35	2.85	0.0107	1.00
CU-047	893.0	860.0	3.70	1.30	0.0046	0.90
CU-070	3025.2	3029.0	0.13	1.00	0.0037	0.70
CU-100	2810.0	2835.0	2.80	0.97	0.0042	0.68
CU-150	2607.6	2618.0	0.40	0.30	0.0009	0.60
SU-017	2090.0	2083.0	0.30	8.00	0.0231	0.90
SU-022	1242.0	1239.0	0.30	0.90	0.0029	0.70
SU-029	1106.0	1130.0	2.10	0.00	0.0000	0.60
SU-040	2311.5	2337.0	1.10	1.95	0.0073	0.50
SU-070	3401.1	3518.0	3.44	0.00	0.0000	0.40
SU-150	3061.5	3100.0	1.26	0.00	0.0000	0.40
SS-040-050(3)	2727.6	2741.0	0.49	3.00	0.0113	1.00
SS-040-050(4)	2902.6	2885.0	0.61	3.50	0.0132	1.00
SS-040-100(4)	2463.1	2476.0	0.52	2.50	0.0094	0.55
SS-070-093(2)	3744.5	3745.0	0.01	0.70	0.0026	0.40
SS-070-093(3)	3855.3	3862.0	0.17	1.00	0.0037	0.45
SS-070-093(4)	3807.3	3812.0	0.12	1.10	0.0040	0.45
SS-070-140(3)	3610.1	3609.0	0.03	0.45	0.0017	0.55
SS-070-140(4)	3596.3	3568.0	0.78	0.60	0.0022	0.50
SS-070-187(3)	3457.0	3465.0	0.23	0.46	0.0017	0.45
SS-070-187(4)	3507.1	3541.0	0.97	0.43	0.0016	0.55
SS-150-050(2)	3184.2	3213.0	0.90	0.45	0.0013	0.60
SS-150-100(2)	3104.7	3092.0	0.41	0.10	0.0003	0.30

umns do not show the degrading effect significantly. However, when k_3 is small (say $k_3<0.7$), the axial force-axial strain curves of the CFT columns do show the degrading effect. This degrading phenomenon again is more prominent with smaller values of k_3.

Comparing Fig. 8 with Fig. 5, we can observe that for the same width-to-thickness ratio, the values of the lateral confining

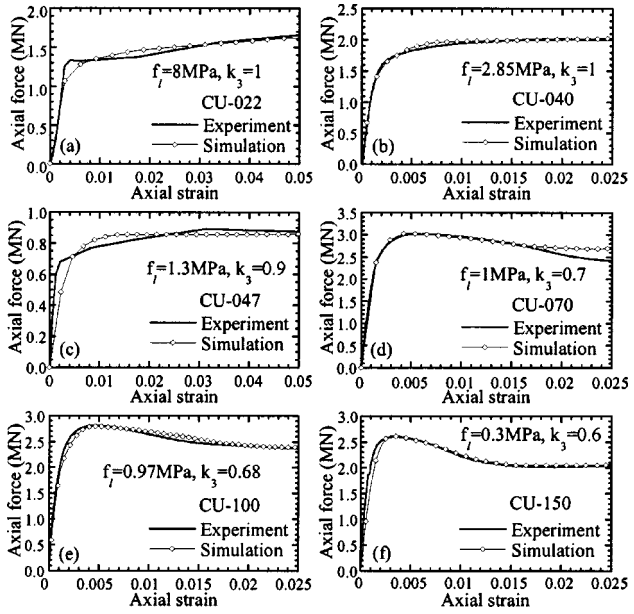

Fig. 5. Axial force versus axial strain for CFT columns with a CU section

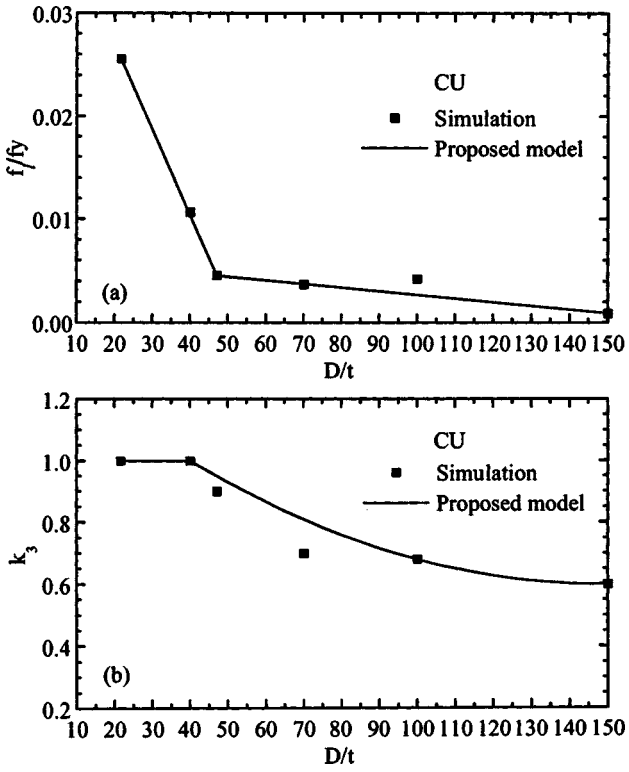

Fig. 6. f_l/f_y and k_3 versus D/t for CFT columns with a CU section

J. Struct. Eng. 2003.129:1322-1329.

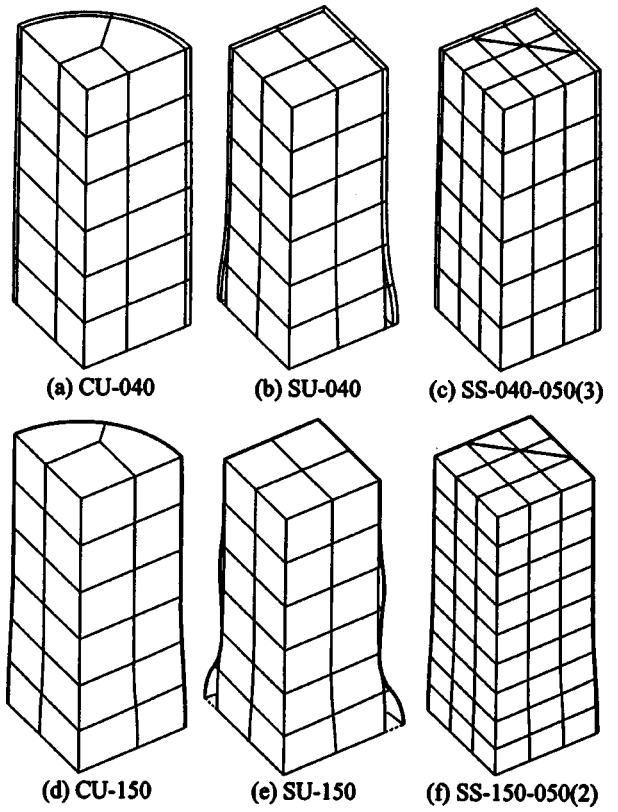

Fig. 7. Deformation shapes of CFT columns

pressure f_l/f_y and the material degradation parameter k_3 for the CFT columns with a SU section are usually less than those for the CFT columns with CU section. This reflects the fact that confining pressure is less and material degradation is greater for square columns than for circular ones. This is because for square columns, the lateral confining pressure is not uniformly applied to the concrete surface. As a result, the concrete core and steel tube

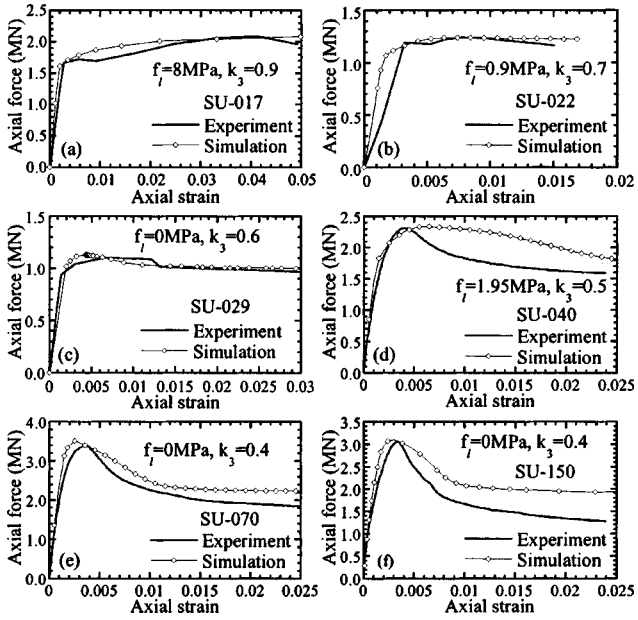

Fig. 8. Axial force versus axial strain for CFT columns with a SU section

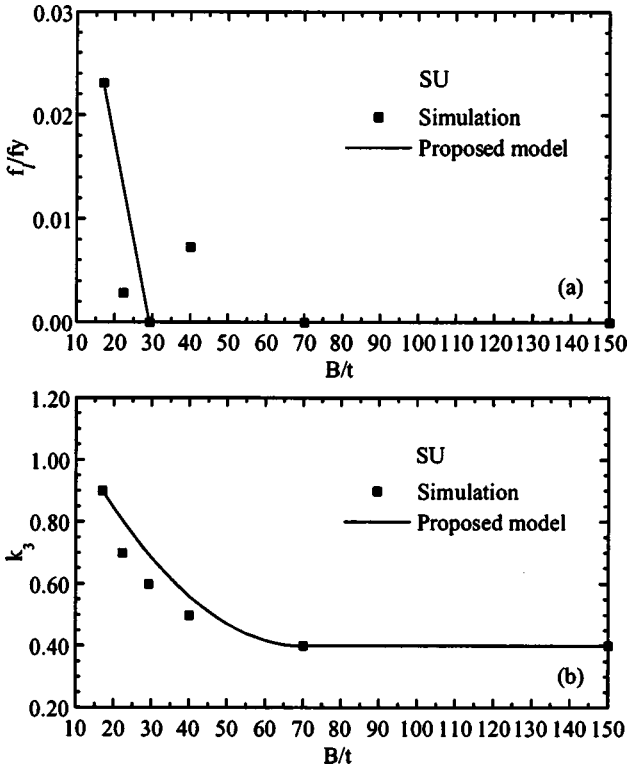

Fig. 9. f_l/f_y and k_3 versus B/t for CFT columns with a SU section

cannot contact firmly to each other and local buckling of the tube may take place. This phenomenon is more obvious by examining the deformation shapes of the SU-040 [Fig. 7(b)] and SU-150 [Fig. 7(e)] columns at the values of axial compressive strains very close to 0.025. It can be observed that due to local buckling, several parts of the tube are separated from the concrete core. This reduces the confining pressure on concrete significantly and causes the concrete strength to degrade easily. For columns with large B/t ratios (say SU-150), the lateral confining pressure f_l may reduce to zero and the material degradation parameter dropped to 0.4. Comparing Fig. 7(b) with Fig. 7(e), we can conclude that the SU CFT columns with large B/t ratios are more prone to have local buckling than those with small B/t ratios.

Figs. 9(a and b) show the values of f_l/f_y and k_3 versus B/t ratio for CFT columns with a SU section, respectively. From the results of numerical simulations, two empirical equations may be proposed for f_l/f_y as follows:

$$f_l/f_y = 0.055048 - 0.001885(B/t) \quad (17 \leqslant B/t \leqslant 29.2) \tag{10a}$$

$$f_l/f_y = 0 \qquad (29.2 \leqslant B/t \leqslant 150) \tag{10b}$$

Again, Eqs. (10*a*) and (10*b*) are formed by two straight lines connecting the data points at $B/t = 17$, 29 and $B/t = 29$, 150 [Fig. 9(a)]. For the parameter k_3, another two empirical equations may be proposed as follows:

$$k_3 = 0.000178(B/t)^2 - 0.02492(B/t) + 1.2722 \quad (17 \leqslant B/t \leqslant 70) \tag{11a}$$

$$k_3 = 0.4 \qquad (70 \leqslant B/t \leqslant 150) \tag{11b}$$

in which Eq. (11*a*) is a parabola passing through the data points at $B/t = 17$, 70 with its vertex being the point $B/t = 70$. Eq. (11*b*) is a horizontal line connecting the data points at $B/t = 70$, 150 [Fig. 9(b)].

J. Struct. Eng. 2003.129:1322-1329.

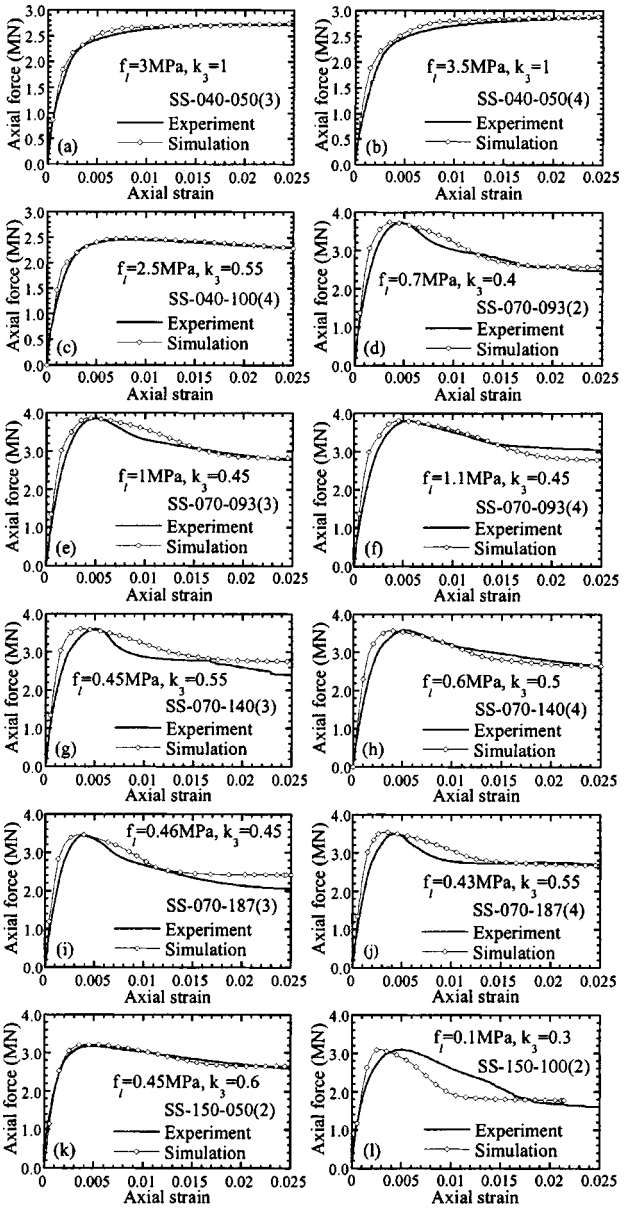

Fig. 10. Axial force versus axial strain for CFT columns with a SS section

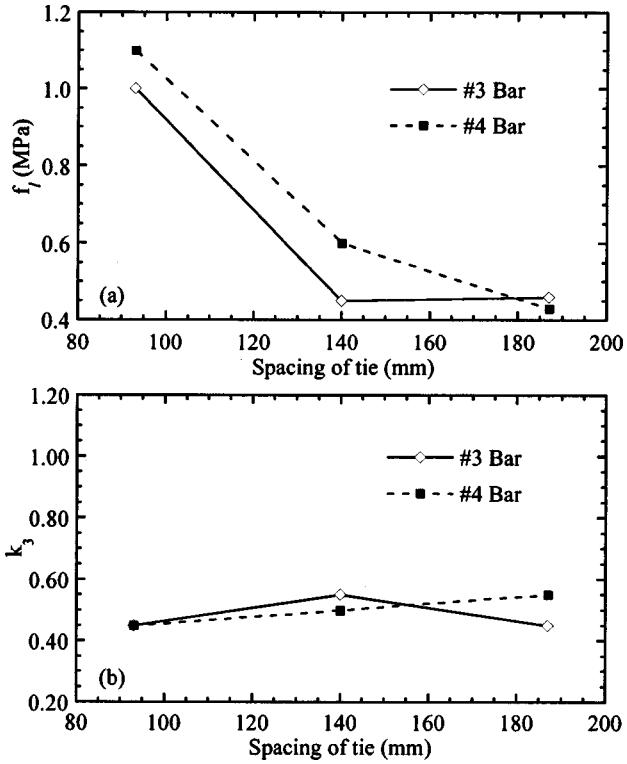

Fig. 11. Influence of tie spacing and tie number on f_l and k_3 for SS-070 CFT columns

Simulations of Concrete-Filled Tubes Columns with SS Section

The results of numerical simulations for CFT columns with a SS section are given in Table 2 and the curves of axial force versus axial strain for these columns are plotted against the experiment data in Fig. 10. Generally, the numerical results show good agreement with the experimental data. Similarly to the columns with CU and SU sections, both the lateral confining pressure f_l and the material degradation parameter k_3 decrease with an increase of width-to-thickness ratio B/t. Comparing Fig. 10(e) with Figs. 8(e) and 5(d), it is observed that the value of f_l for the SS-070-093(3) column is higher than that for the SU-070 column. This is because the use of reinforcing ties prevents the local buckling of steel tube and enhances the lateral confining pressure of the square tubes. However, the lateral confining pressure of the stiffened square column is still less than that of a circular one. As a result, the material degradation parameter k_3 for columns with SS sections would be higher than that for columns with a SU section but lower than that for columns with a CU section.

Figs. 7(c and f) show the deformation shapes of the SS-040-050(3) and SS-150-050(2) columns at the values of axial compressive strains very close to 0.025. It can be observed that local buckling of the tube is totally prevented by the reinforcing ties not only for columns with small B/t ratios but also for columns with large B/t ratios. Fig. 11(a) plots f_l versus tie spacing and tie number for SS-070 columns. From the figure, it can be concluded that the lateral confining pressure decreases with an increase in tie spacing. In addition, with the same tie spacing, the column having larger reinforcing tie number (larger diameter) would have larger lateral confining pressure. Fig. 11(b) plots k_3 versus tie spacing and tie number for SS-070 columns. From the figure, it can be concluded that as long as reinforcing ties are used, the influence of tie spacing and bar number on k_3 is not significant.

Conclusions

In this paper, nonlinear finite element analyses of CFT columns with CU, SU and SS sections are analyzed. Based on the numerical results, the following conclusions may be drawn:

1. For CFT columns with a CU section, the tubes can provide a good confining effect to concrete especially when the width-to-thickness ratio is small (say $D/t<40$). Local buckling of the steel tube is not likely to occur. Recent research on local buckling of CFT columns might shed more light on the delineation (Bradford, Loh, and Uy 2002).
2. For CFT columns with a SU section, the tubes do not provide a large confining effect to concrete especially when the width-to-thickness ratio is large (say $B/t>30$). Local buckling of the steel tube is very likely to take place.

J. Struct. Eng. 2003.129:1322-1329.

3. The confining effect of CFT columns with a SS section is enhanced by the use of reinforcing ties especially when the tie spacing is small and the tie number (or tie diameter) is large. Local buckling of steel tube is prevented by the reinforcing tie and is less likely to occur.
4. Both the lateral confining pressure f_l and the material degradation parameter k_3 decrease with an increase in width-to-thickness ratio (D/t or B/t). When the width-to-thickness ratio is small, f_l and k_3 tend to be large due to the lateral confinement from the steel tube. When the width-to-thickness ratio is large, f_l and k_3 tend to be small due to the lack of lateral support from the tube.

Acknowledgment

This research work was financially supported by the National Science Council, Republic of China under Grant No. NSC 89-2711-3-319-200-37.

References

American Concrete Institute (ACI). (1999). ''Building code requirements for structural concrete and commentary.'' *ACI 318-99*, Detroit.

ASCE. (1982). *ASCE task committee on concrete and masonry structure, state of the art report on finite element analysis of reinforced concrete*, ASCE, New York.

Boyd, F. P., Cofer, W. F., and McLean, D. (1995). ''Seismic performance of steel-encased concrete column under flexural loading.'' *ACI Struct. J.*, 92(3), 355–365.

Bradford, M. A. (1996). ''Design strength of slender concrete-filled rectangular steel tubes.'' *ACI Struct. J.*, 93(2), 229–235.

Bradford, M. A., Loh, H. Y., and Uy, B. (2002). ''Slenderness limits for filled circular steel tubes.'' *J. Constr. Steel Res.*, 58(2), 243–252.

El-Tawil, S., and Deierlein, G. G. (1999). ''Strength and ductility of concrete encased composite columns.'' *J. Struct. Eng.*, 125(9), 1009–1019.

Furlong, R. W. (1967). ''Strength of steel-encased concrete beam columns.'' *J. Struct. Div. ASCE*, 93(5), 113–124.

Furlong, R. W. (1974). ''Concrete encased steel columns—Design tables.'' *J. Struct. Div., ASCE*, 100(9), 1865–1882.

Ge, H. B., and Usami, T. (1992). ''Strength of concrete-filled thin-walled steel box columns: Experiment.'' *J. Struct. Eng.*, 118(11), 3036–3054.

Ge, H. B., and Usami, T. (1994). ''Strength analysis of concrete-filled thin-walled steel box columns.'' *J. Constr. Steel Res.*, 30(3), 259–281.

Hajjar, J. F., and Gourley, B. C. (1996). ''Representation of concrete-filled steel tube cross-section strength.'' *J. Struct. Eng.*, 122(11), 1327–1336.

Hibbitt, Karlsson, and Sorensen, Inc. (2000). *ABAQUS theory manual and user manuals, Version 5.8*, Providence, R.I.

Huang, C. S., et al. (2002). ''Axial load behavior of stiffened concrete-filled steel columns.'' *J. Struct. Eng.*, 128(9), 1222–1230.

Hu, H.-T., and Schnobrich, W. C. (1989). ''Constitutive modeling of concrete by using nonassociated plasticity.'' *J. Mater. Civ. Eng.*, 1(4), 199–216.

Knowles, R. B., and Park, R. (1969). ''Strength of concrete filled steel tubular columns.'' *J. Struct. Div., ASCE*, 95(12), 2565–2587.

Liang, Q. Q., and Uy, B. (2000). ''Theoretical study on the post-local buckling of steel plates in concrete-filled box column.'' *Comput. Struct.*, 75(5), 479–490.

Mander, J. B., Priestley, M. J. N., and Park, R. (1988). ''Theoretical stress-strain model for confined concrete.'' *J. Struct. Eng.*, 114(8), 1804–1826.

Morino, S. (1998). ''Recent developments in hybrid structures in Japan—Research, design and construction.'' *Eng. Struct.*, 20(4–6), 336–346.

Richart, F. E., Brandtzaeg, A., and Brown, R. L. (1928). ''A study of the failure of concrete under combined compressive stresses.'' *Bull. 185*, Univ. of Illinois Engineering Experimental Station, Champaign, Ill.

Saenz, L. P. (1964). ''Discussion of 'Equation for the stress-strain curve of concrete' by P. Desayi, and S. Krishnan.'' *ACI J.*, 61, 1229–1235.

Schneider, S. P. (1998). ''Axially loaded concrete-filled steel tubes.'' *J. Struct. Eng.*, 124(10), 1125–1138.

Shams, M., and Saadeghvaziri, M. A. (1997). ''State of the art of concrete-filled steel tubular columns.'' *ACI Struct. J.*, 94(5), 558–571.

Uy, B. (1998). ''Local and post-local buckling of concrete filled steel welded box columns.'' *J. Constr. Steel Res.*, 47(1–2), 47–72.

Wu, M.-H. (2000). ''Numerical analysis of concrete filled steel tubes subjected to axial force.'' MS thesis, Dept. of Civil Engineering, National Cheng Kung Univ., Tainan, Taiwan, R.O.C.

Zhang, W., and Shahrooz, B. M. (1999). ''Comparison between ACI and AISC for concrete-filled tubular columns.'' *J. Struct. Eng.*, 125(11), 1213–1223.